



19 events. The potential for simulating future hourly precipitation by associating historic hourly  
20 precipitation patterns with PCE's and monthly temperature is assessed.

21 *Key words:* precipitation analysis, weather type categorization, GCM temperature, hourly precipitation,  
22 average monthly temperature, pressure change event, probability of precipitation, extreme event

## 23 1. Introduction

24 Global climate variability and change is largely caused by modifications to the global energy and water  
25 cycles. To improve our ability to adapt to precipitation changes under global warming (Trenberth, Dai et  
26 al. 2003), research is necessary to characterize the relationship between precipitation and temperature  
27 (Trenberth 1998, Trenberth, Dai et al. 2003, Allan and Soden 2007, Neiman., Ralph. et al. 2008, Lenderink  
28 and van Meijgaard 2010). This relationship is complex, as it varies over space and time. Although  
29 General Circulation Models (GCMs) can generally investigate coarser temporal scales (e.g. annual or  
30 decadal) in larger geographic areas (e.g. Northeast US, global), more uncertainties are observed at smaller  
31 temporal and spatial scales, since local climate is also influenced by local geography, land cover, and  
32 related circulation patterns (Mitchell, Johns et al. 1999, Räisänen 2001, Zveryaev and Allan 2005,  
33 Sorteberg and KvamstØ 2006).

34 Researchers have tried to link these two factors using physical and atmospheric explanations. For  
35 example, Trenberth, Dai et al. (2003) suggested that through convection, the moisture required for  
36 precipitation is drawn from an area of atmosphere that is about four times the rainy area. A 7% increase  
37 in air moisture holding per degree of warming at the local level has been used to imply a similar rate of  
38 global precipitation change, based on the Clausius–Clapeyron relation (Trenberth and Shea 2005, Sun,  
39 Solomon et al. 2007). Other studies investigate this relationship at different time scales, from monthly  
40 (Trenberth and Shea 2005, King, Klingaman et al. 2014) to daily (Sun, Solomon et al. 2007, Westra,  
41 Alexander et al. 2013) and sub-daily (Lenderink and van Meijgaard 2008, Lenderink and van Meijgaard  
42 2010); still others explore this relationship based on differences in precipitation patterns, looking at means  
43 (Allen and Ingram 2002, Trenberth 2011), extremes (Groisman, Knight et al. 2005, Meehl, Arblaster et al.  
44 2005, Shaw, Royem et al. 2011, Meehl, Washington et al. 2012, Kunkel, Karl et al. 2013), and events of  
45 varying durations (Panthou, Mailhot et al. 2014, Wasko, Sharma et al. 2015).

46 For example, Madden and Williams (1978) found a frequent negative correlation between precipitation  
47 and summer air temperature at time scales ranging from inter-annual to multi-decadal in the contiguous  
48 United States and Europe. Zhao and Khalil (1993) confirmed a similar negative correlation in the summer,  
49 after exploring monthly data of the contiguous United States from 1905 to 1984. However, on days with  
50 mean daily temperatures in excess of 12 °C, Lenderink and van Meijgaard (2008) found that the  
51 probability of one-hour precipitation extremes in De Bilt, Netherlands increased much faster than the  
52 Clausius–Clapeyron relation suggests, extending this finding to larger European simulations.

53 In general, projections from GCMs are used to interpret the relationship between precipitation and  
54 temperature at coarser temporal scales (e.g. annual or decadal) under climate change scenarios when  
55 considering larger geographic areas (e.g. Northeast US, global). Yet, precipitation datasets at fine time  
56 scales (e.g. hourly or sub-hourly) are required to study the potential impacts of climate change on water  
57 resource management, urban hydrology, and agriculture. For example, one of the two primary causes of  
58 runoff is Hortonian excess precipitation, whereby runoff is generated instantaneously whenever the  
59 intensity of precipitation exceeds the infiltration capacity of the land surface. To assess whether  
60 precipitation will be more intense under climate change, and possibly increase runoff generation,  
61 precipitation sequences downscaled from GCM projections are needed at fine temporal scales. Despite  
62 the dynamic methods used by Regional Climate Models (RCMs), stochastic precipitation generators,  
63 based on downscaled GCM projections, have been developed as an alternative (Fowler, Blenkinsop et al.  
64 2007, Wilks 2010) and used extensively for flood risk management (Haberlandt, von Eschenbach et al.  
65 2008), sizing reliable rainwater harvesting systems (Basinger, Montalto et al. 2010), and other water  
66 resource management tasks (Shamir, Megdal et al. 2015). Stochastic precipitation generators create long  
67 continuous Markovian sequences of precipitation through a variety of methods (Wilks and Wilby 1999).  
68 One technique for sequence generation uses samples from parameterized statistical distributions of wet-  
69 day rain volume (Stern and Coe 1984, Wilks 1998), arrival and cell conditions intensity and duration

70 (Rodriguez-Iturbe, Cox et al. 1987, Rodriguez-Iturbe, Cox et al. 1988, Wasko, Pui et al. 2015, Wasko and  
71 Sharma 2017), and event characteristics (Heneker, Lambert et al. 2001); another relies on non-  
72 parametrically sampling historical observations (Lall, Rajagopalan et al. 1996, Lall and Sharma 1996,  
73 Sharma and Lall 1999, Basinger, Montalto et al. 2010) with a moving window to preserve seasonality  
74 (Rajagopalan, Lall et al. 1996).

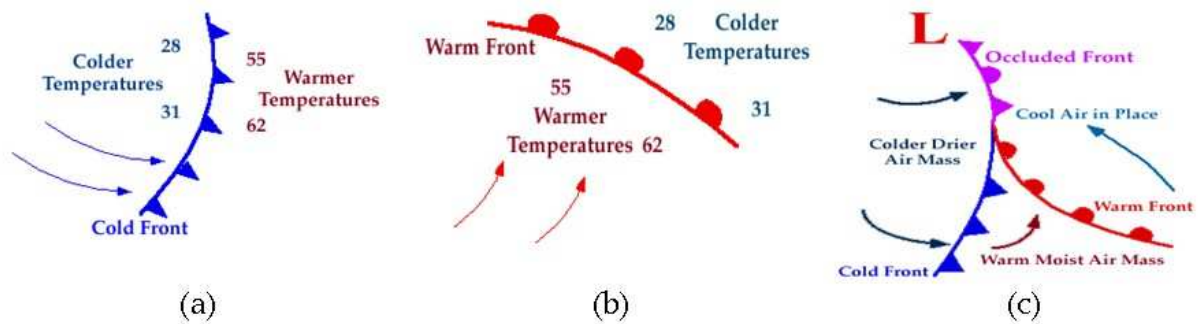
75 The quality of downscaled GCM precipitation datasets is contingent upon accurate temperature  
76 predictions and a strategy for minimizing prediction bias (Johnson and Sharma 2009, Johnson and  
77 Sharma 2012). Researchers found that pressure and temperature have the most agreement across the  
78 GCMs (Johnson and Sharma 2009), while precipitation has the least consensus (Kendon, Rowell et al. 2008,  
79 Johnson and Sharma 2009) . A better understanding of the relationship between precipitation and  
80 temperature is necessary to increase confidence in precipitation projections derived from other GCM  
81 projections, such as monthly temperature.

82 This paper explores how fine temporal scale (e.g. hourly) precipitation patterns are related to coarser  
83 temporal scale (e.g. average monthly) temperature. The physical causes of precipitation in a free  
84 atmosphere system are discussed first. Next, an investigation into the relationship of air pressure and  
85 precipitation is explored both at hourly time steps, and on an event basis. This analysis is then extended  
86 to examine how event based precipitation characteristics are impacted by Average Monthly Temperature  
87 (AMT). The results are used to discuss the potential development of a new stochastic precipitation  
88 generator that produces synthetic hourly precipitation time series by non-parametrically resampling  
89 historical observations, informed by GCM projections of AMT, among other variables.

## 90 2. Mechanisms of Precipitation

91 One of the key causes of precipitation is the condensation of air that ascends as it moves laterally over  
92 irregular terrain (orographic lifting) or is physically displaced by atmospheric phenomena (e.g. via frontal  
93 lifting) (Bjerknes and Kristiania 1922). Condensed moisture then falls to the ground as precipitation after  
94 drops coalesce enough to overcome the forces of drag (Ahrens, Jackson et al. 2012).

95 In a free atmosphere, the primary cause of condensation is the displacement of air masses (Bjerknes and  
96 Kristiania 1922). The earliest researcher describing precipitation generated from the frontal movement of  
97 air masses was Bjerknes and Kristiania (1923), who studied atmospheric circulation patterns. There are  
98 three main categories of frontal precipitation (Bjerknes and Kristiania 1922, Bjerknes and Kristiania 1923):  
99 (1) A cold front forms when cold, dry stable air masses lift and replace relatively unstable, warm, moist  
100 air masses previously found near the land surface. Typically, the cold air moves from the northwest to  
101 southeast direction in the northern hemisphere. The cold air forces its way under the warm air, which is  
102 then convected upward, where it cools, condenses, and coalesces, often causing short-duration, high-  
103 intensity precipitation. (2) By contrast, a warm front is formed by the advance of a warm moist air mass  
104 and the simultaneous slow retreat of cold dry air. Most commonly, warm air moves from the southeast to  
105 the northwest in the northern hemisphere. Since warm air has a lower density, it rolls up and over the  
106 cold air and can cause light to moderate precipitation over a large geographic area. (3) Occludal fronts  
107 occur when cold and warm fronts collide, causing a cyclone with low pressure in the joint area. Occludal  
108 fronts typically move to the northeast, and cause synoptic (because both warm and cold fronts are  
109 present) precipitation over large land areas. Figure 1 graphically illustrates the three types of fronts.



110

111 **Figure 1 Air mass front types (the numbers in plot indicate temperature in Fahrenheit) (a) Cold front,**  
 112 **blue arrows indicate the direction of movement, (b) Warm front, red semi-cycles indicate the direction**  
 113 **of movement, (c) Occluded front, purple arrows and semi-cycles show the direction of move, both cold**  
 114 **front and warm front move counter-clockwise and produce low pressure region in the joint area.**  
 115 **(Urbana-Champaign 2010)**

116 Ahrens, Jackson et al. (2012) summarized general relationships between precipitation, temperature, and  
 117 pressure for each of the three types of fronts (Table 1). Note that the trends in temperature changes are  
 118 not consistent for all front types, especially for the Occluded front, which makes it difficult to develop a  
 119 direct relationship between temperature and precipitation. However, when air is lifted by any of the three  
 120 different frontal mechanisms, air pressure at the ground surface is consistently reduced (Hughes and  
 121 Mayes 2014). This phenomenon is well-documented at the synoptic scale, as a result of frontal  
 122 precipitation (Urbana-Champaign 2010). At the local or meso-scale, Hoxit, Chappell et al. (1976) found  
 123 that surface pressure dropped due to the formation of convective clouds, triggering showery storms. The  
 124 magnitude of the pressure drop is associated with the type of air mass movement at the synoptic scale or  
 125 with the extent of the surface heating imbalance at the meso-scale, suggesting that in both cases pressure  
 126 changes may provide a potential physical link between precipitation and seasonal variable frontal  
 127 movements, related to AMT and atmosphere stability.

128

	Before Passing	While Passing	After Passing
<b>Temperature</b>	warm	sudden drop	steadily dropping
<b>Pressure</b>	falling steadily	minimum, then sharp rise	rising steadily
<b>Precipitation</b>	short period of showers	heavy rains, sometimes with hail, thunder and lightning	showers then clearing

(a)

	Before Passing	While Passing	After Passing
<b>Temperature</b>	cool-cold, slow warming	steady rise	warmer, then steady
<b>Pressure</b>	usually falling	leveling off	slight rise, followed by fall
<b>Precipitation</b>	light-to-moderate rain, snow, sleet, or drizzle	drizzle or none	usually none, sometimes light rain or showers

(b)

	Before Passing	While Passing	After Passing
<b>Temperature</b> •Cold occluded •Warm occluded	Cold or cool Cold	Dropping Rising	Colder Milder
<b>Pressure</b>	Usually falling	Low point	Usually rising
<b>Precipitation</b>	Light, moderate, or heavy precipitation	Light, moderate, or heavy continuous precipitation or showers	Light-to-moderate precipitation followed by general clearing

(c)

129 **Table 1 Climate characteristic effect of three front types a) Cold front, b) Warm front, c) Occludal front**  
130 **(Urbana-Champaign 2010)**

### 131 3. Data and Methods

#### 132 3.1 Data

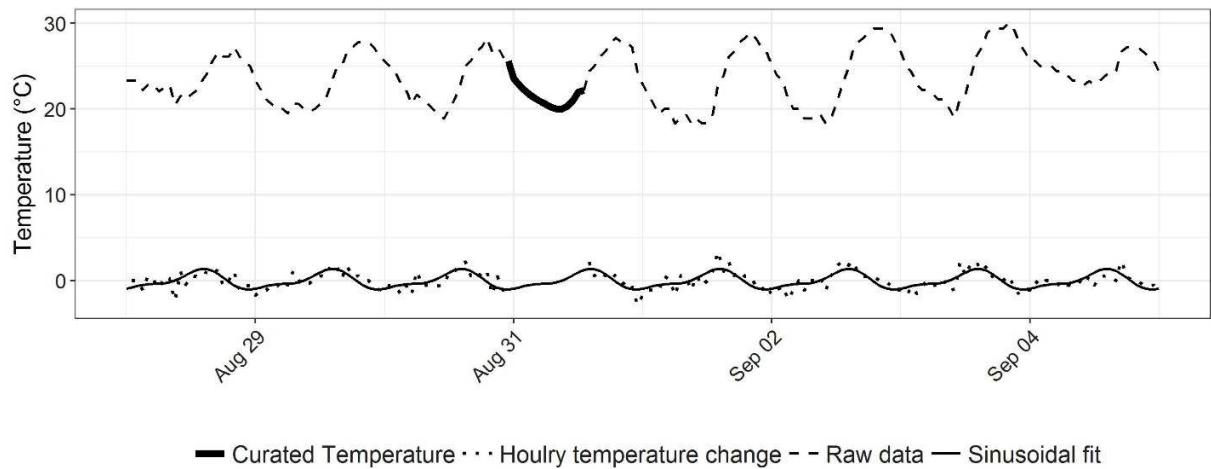
133 The analysis focuses on the northeastern coastal United States, a region extending from Philadelphia to  
134 Boston, and characterized by plains with no high mountains. In this region, other than the general surface  
135 heating mechanism for local summer storms, the vertical movement of air masses is typically associated  
136 with frontal precipitation, rather than orographic lifting. Studies describing the relationship between  
137 precipitation and temperature (Lenderink and van Meijgaard 2010, Shaw, Royem et al. 2011, Panthou,  
138 Mailhot et al. 2014, Wasko and Sharma 2017) use data from many locations to prove the geographical  
139 representative of their statistics. However, the physical mechanism of precipitation formation in this  
140 study area has been observed in many other locations around the world (Hoxit, Chappell et al. 1976,



141 Knupp and Cotton 1985, Neiman., Ralph. et al. 2008, Adams-Selin and Johnson 2010, Ahrens 2012, Dawn  
142 and Mandal 2014, Houze, Rasmussen et al. 2015). The data used in this study includes hourly  
143 observations of temperature, sea level air pressure, and precipitation from the international airports in  
144 New York City, Philadelphia and Boston from 1948 to 2011.

145 Since the topography and climate across the region are known to be similar, data from the three cities,  
146 spanning over a distance of 480 km, are pooled for this analysis. More frequent extreme precipitation in  
147 the future has been projected for this region by other researchers (Hayhoe, Wake et al. 2008, Demaria,  
148 Palmer et al. 2016, USGCRP 2017). The pooling increases the number of data points that can be used in  
149 the analysis, especially for the extremes.

150 Because 1.04% of all time steps in the historical data contains some gaps, (i.e. missing data, cumulative  
151 period with no detailed information, the time-interval of observation is longer than one hour for several  
152 decades, etc.), an interpolation method is developed to fill in the missing data points for gaps less than 24  
153 hours. A moving average method, with a window width of a single day, is used to smooth out gaps of  
154 less than six hours (1.03%). For gaps between six hours and 24 hours (0.01%), a 2<sup>nd</sup> harmonic function is  
155 fitted to the values of the dry days (all gaps are treated as dry), with a length of one week (adjustable)  
156 centered on the day of interest and adjusted to match the values of the gap's end points. Then, using this  
157 adjusted harmonic function, the gaps were filled with values that mimic the general change pattern for  
158 the neighboring days and which connect smoothly to the observed data. Figure 2 illustrates a sample of  
159 such a case. This method is applied on both temperature and air pressure. Where longer gaps (greater  
160 than 24 hours) were evident, data was eliminated from the analysis.



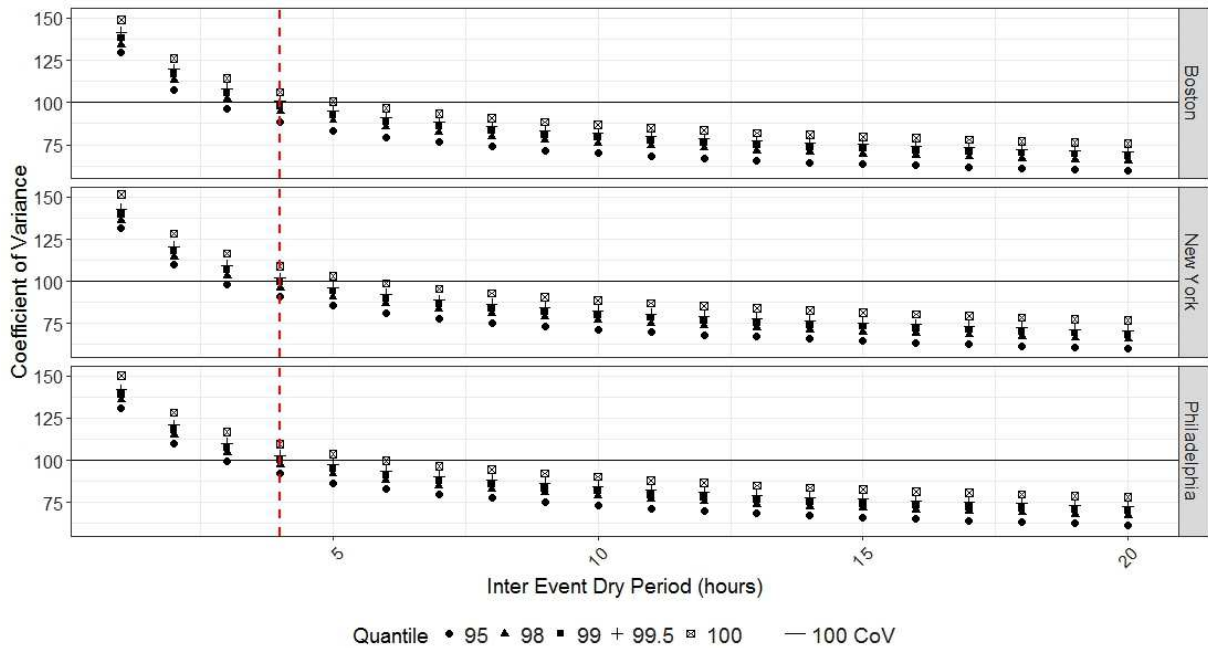
161

162

**Figure 2 Sample of missing data filling**

163 **3.2 Methods**

164 Because the movement of air masses is typically associated with pressure changes, the first step in the  
 165 analysis was to investigate the pressure changes associated with precipitation. For the purposes of this  
 166 paper, both pressure change and precipitation were investigated on an event basis. Precipitation events  
 167 were defined by an Inter-Event Dry Period (IntEDP). Based on Restrepo-Posada and Eagleson (1982),  
 168 IntEDP follows an exponential distribution for which the mean equals the standard deviation, or  
 169 Coefficient of Variation (CV) of unity. However, the historic IntEDP is affected by extreme events, which  
 170 dramatically affect calculations of the CV. In Figure 3, the CV for each city is calculated and plotted based  
 171 on IntEDP quantile thresholds of 95%, 98%, 99%, 99.5% and 100%. An IntEDP beyond each threshold is  
 172 not included in the calculations. Based on the results, the CV is sensitive to the extreme events in the  
 173 distribution tail (e.g. the 100% results are far from 99.5% results, especially for the short IntEDPs). To  
 174 avoid the influence of these low-frequency events (e.g. 0.5% for 99.5% quantile threshold), this paper uses  
 175 99.5% as the quantile threshold to determine the minimum IntEDP, which is four hours for all cities  
 176 (Figure 3).



177

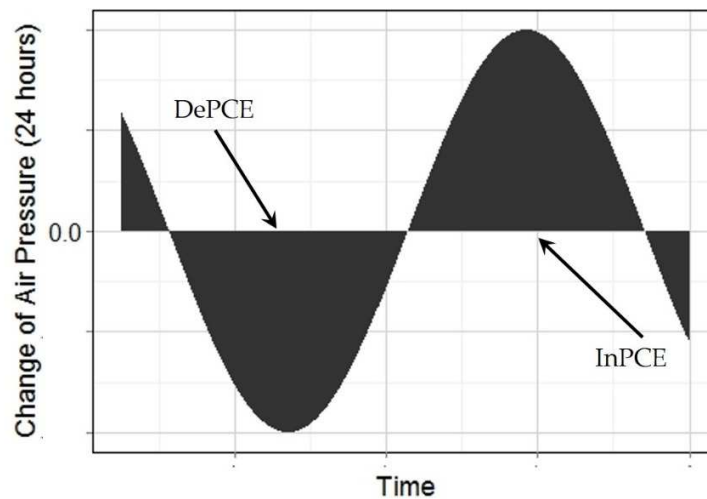
178 **Figure 3 Analysis of IntEDP, black horizontal solid line (CV of unity), red vertical dash line (4 hour**  
 179 **IntEDP)**

180 A Pressure Change Event (PCE) is defined using de-seasonalized air pressure. De-seasonalized air  
 181 pressure is the change in air pressure over a 24-hour period, as shown in the following equation.

182 
$$P'(t) = P(t) - P(t - 24)$$

183 Where  $P(t)$  is the actual air pressure on hour  $t$ ,  $P'(t)$  is the de-seasonalized air pressure on hour  $t$ . Two  
 184 different types of PCEs are possible, as shown conceptually in Figure 4. The horizontal axis represents  
 185 time, while vertical axis represents the change in air pressure over 24 hours, i.e. the de-seasonalized air  
 186 pressure series. The shaded areas above the horizontal axis are defined as an Increasing Pressure Change  
 187 Events (InPCEs) because the air pressure increases over time. The shaded areas below the horizontal axis  
 188 are defined as Decreasing Pressure Change Events (DePCEs), because air pressure decreases with time.  
 189 The local maxima and minima in the figure indicate the greatest positive and negative 24-hour changes in  
 190 pressure, respectively. As shown in Figure 4, each PCE, increasing or decreasing, is bracketed by time  
 191 points of stable pressure (e.g. no change over 24 hours). Using the data in this study, InPCEs correspond

192 to Event Pressure Changes (EPC) from 0 to 1100 hPa; DePCE EPCs range from -1200 to 0 hPa. EPC is  
193 defined as the cumulative air pressure change within a PCE. The sample sizes of PCEs for BOS, NYC and  
194 PHL were, respectively, 11564, 7147 and 8511. Based on the meteorology finding described in Table 1,  
195 precipitation is hypothesized to occur more frequently during DePCEs.



196

197

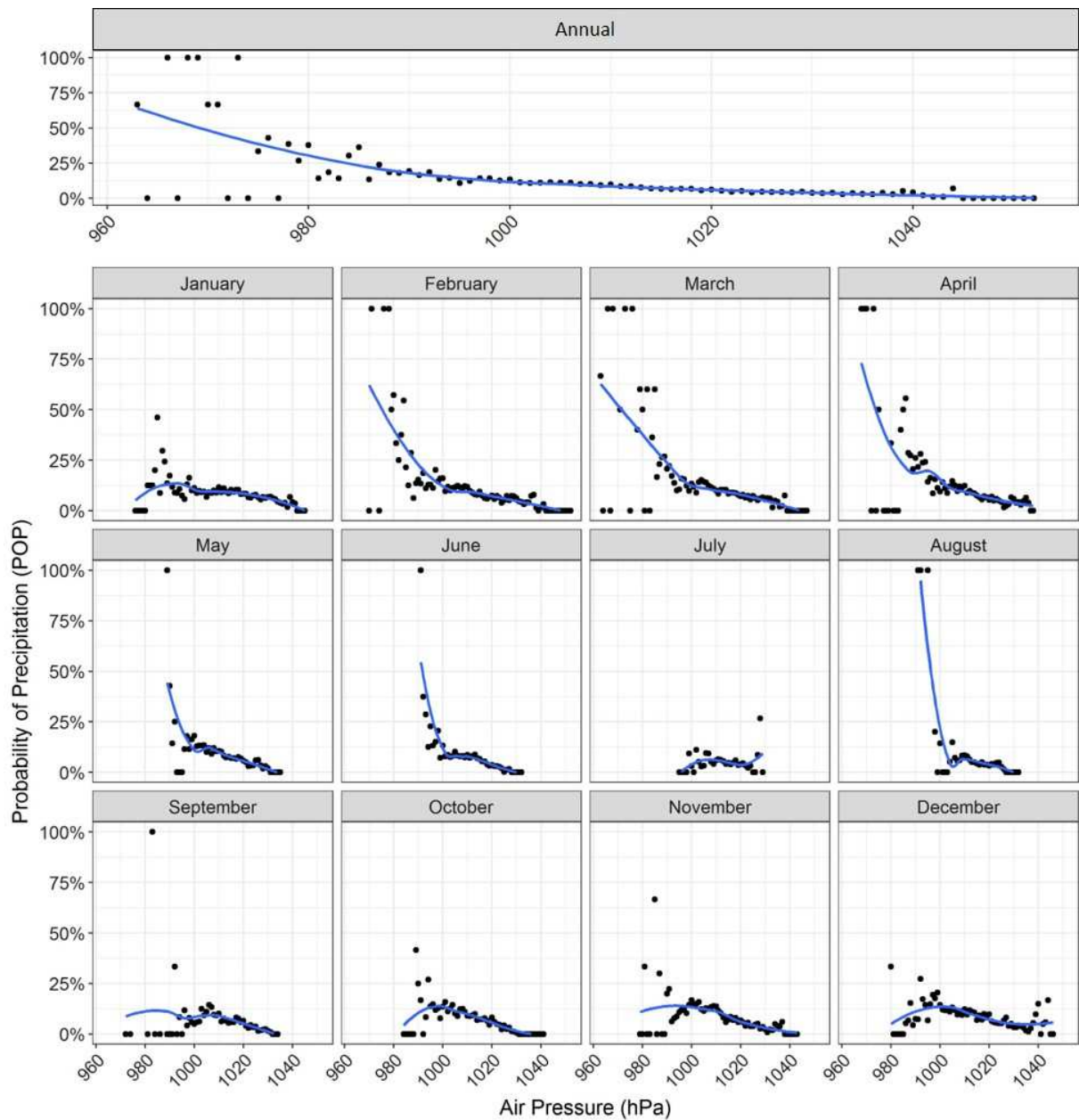
**Figure 4 PCE definition**

198 Next, the relationships between historical hourly precipitation and air pressure were explored. An  
199 exploratory analysis was performed to determine whether air pressure is related to precipitation across  
200 the study area. Hourly Probabilities of Precipitation (POPs) over the full air pressure range for a year and  
201 each month were explored graphically. Then, the association between precipitation occurrence and  
202 pressure change was qualitatively investigated on an event basis. Historical observations were  
203 specifically inspected for coincidences of DePCEs and precipitation. An EPC histogram of both rainy and  
204 non-rainy PCEs was plotted to explore whether precipitation is more frequently triggered during DePCEs.  
205 The association between precipitation and EPC was then further analyzed and quantified in terms of PCE  
206 Precipitation Depth (PD) and PCE POP, with both computed from the total number of rainy PCEs.

207 For the association between precipitation and PCE to be applicable under climate change conditions, it is  
208 hypothesized that atmosphere stability, PCE POP, and PCE PD must be dependents of AMT. To test this  
209 theory, the frequency of PCEs is graphically inspected to interpret the stability of atmospheric system  
210 under different AMT conditions. By importing AMT information, the seasonality, corresponding PD, and  
211 POP of different PCE types is explored. To bridge precipitation and AMT, heatmaps and contours of PCE  
212 POP were overlaid with AMT for different half-years (Jan – June and July – Dec); different PCE PD  
213 percentiles were also investigated against AMT under different EPC magnitudes and seasons.

#### 214 **4. Results and Discussion**

215 Figure 5 displays POP associated with different air pressures for LaGuardia International Airport (NYC)  
216 at an hourly time scale. POP in this chart refers to the probability of any form of precipitation. At the top  
217 of the chart is the POP versus hourly air pressure for the full data set. Below, POP is broken down by  
218 month. The figure indicates that POP is negatively correlated to the hourly air pressure, irrespective of  
219 month. However, during July, August, and September, this trend is less pronounced than during other  
220 months. This trend is likely because 1) the air system is relatively stable in summer, with less variability  
221 in air pressure, and 2) summertime convection storms are often highly localized and may not pass over  
222 the climate station, even it is in the tributary area of the storm's convection. The same trends and  
223 phenomena were also found in Boston and Philadelphia (Figures not shown).

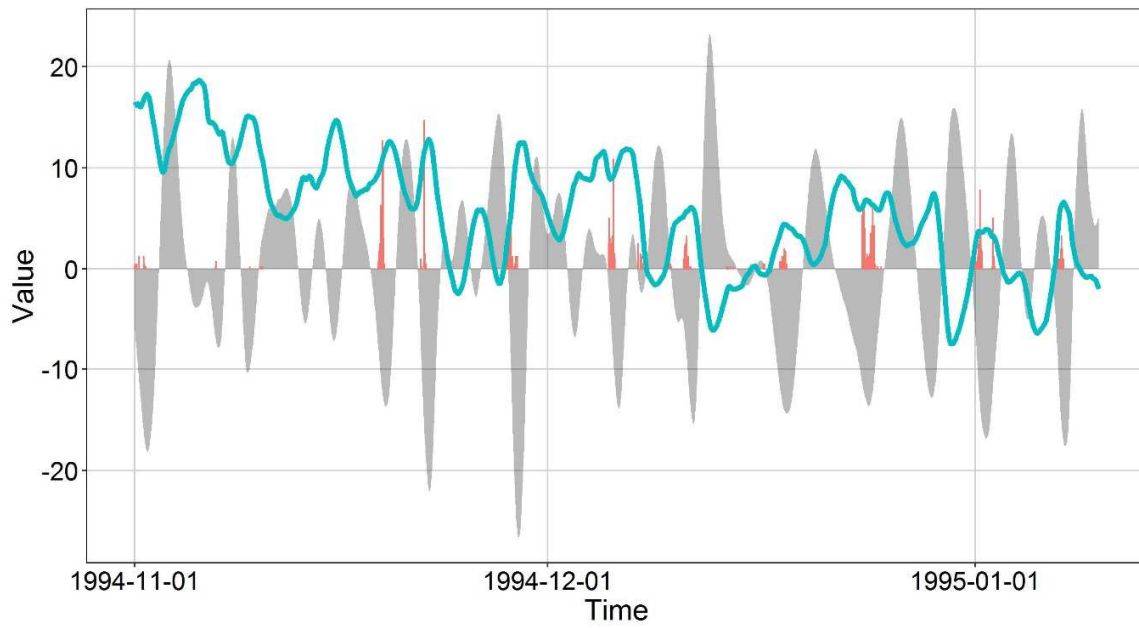


224  
 225 **Figure 5 POP on hourly air pressure in NYC LaGuardia International Airport (the local regressions are**  
 226 **indicated by the blue lines)**

227 Figure 6 shows a sample sequence of alternating PCEs (shaded area) and the associated hyetographs (red  
 228 bars) and 24-hour-smoothed temperature (green line). This graph illustrates that precipitation is generally  
 229 associated with the DePCEs, which supports the trends illustrated in Table 1 (i.e. that frontal precipitation  
 230 is successive to pressure fall).

231 Histograms describing all pooled PCEs (red) and all rain-triggering PCEs (green) are shown in Figure 7.  
232 The rain-triggering PCEs are defined as those PCEs whose durations overlap with the beginning of a  
233 precipitation event. The histogram of the full sample of all PCEs is similar to a normal distribution, with a  
234 mean near zero. The distribution of rain-triggering PCEs is, however, skewed to the left and is  
235 discontinuous at the vertical axis (in the negative range). The left-skewness is consistent with the  
236 meteorological interpretation that as air masses are vertically lifted, negative changes in pressure are  
237 associated with precipitation events. The discontinuity in the distribution could indicate the presence of  
238 two different types of fronts. Cold fronts lift warm air rapidly, generating precipitation over relatively  
239 small geographic areas very soon after the pressure drops. Because POP in the negative region of Figure 7  
240 is higher, it may be that these events correspond to cold-front storms. Alternatively, the smaller POP  
241 under positive EPC may correspond to warm-front storms, since warm-front storms usually affect a large  
242 region ahead of the front. For this reason, precipitation correlated with InPCE has a lower POP.

243

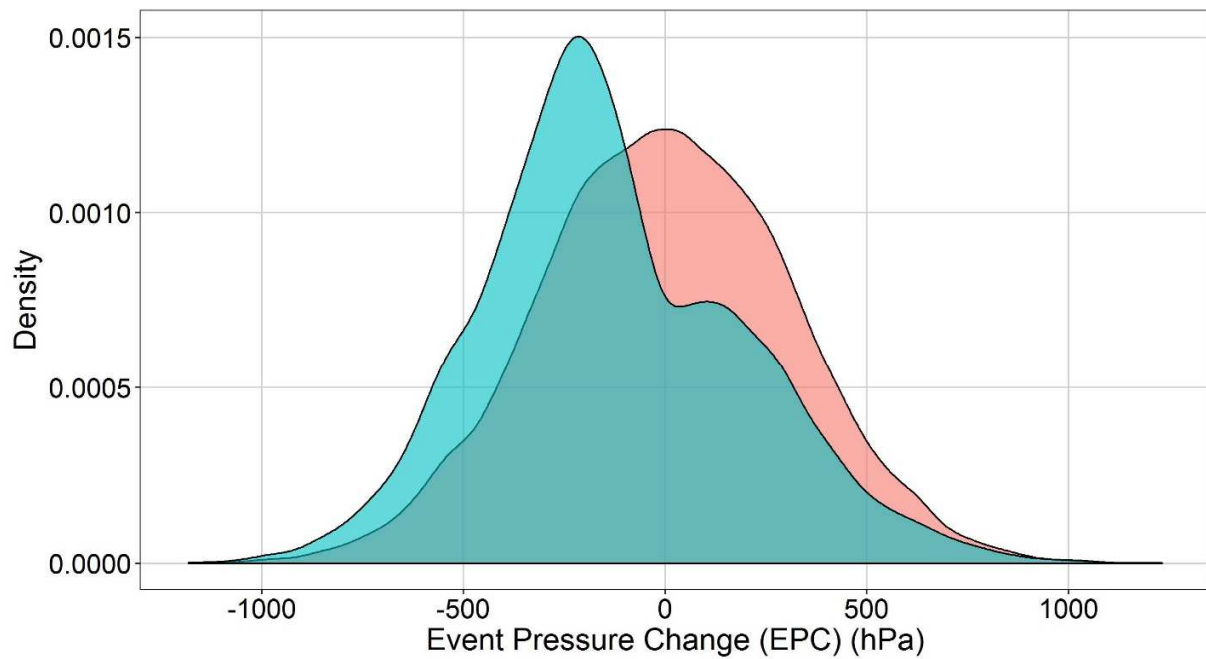


Air pressure change (hPa)
  Precipitation (mm)
  Smoothed Temperature (°C)

244

245

**Figure 6 PCEs and precipitation from 1994-11-01 to 1995-1-10 in BOS**



All PCEs
  Rainy PCEs

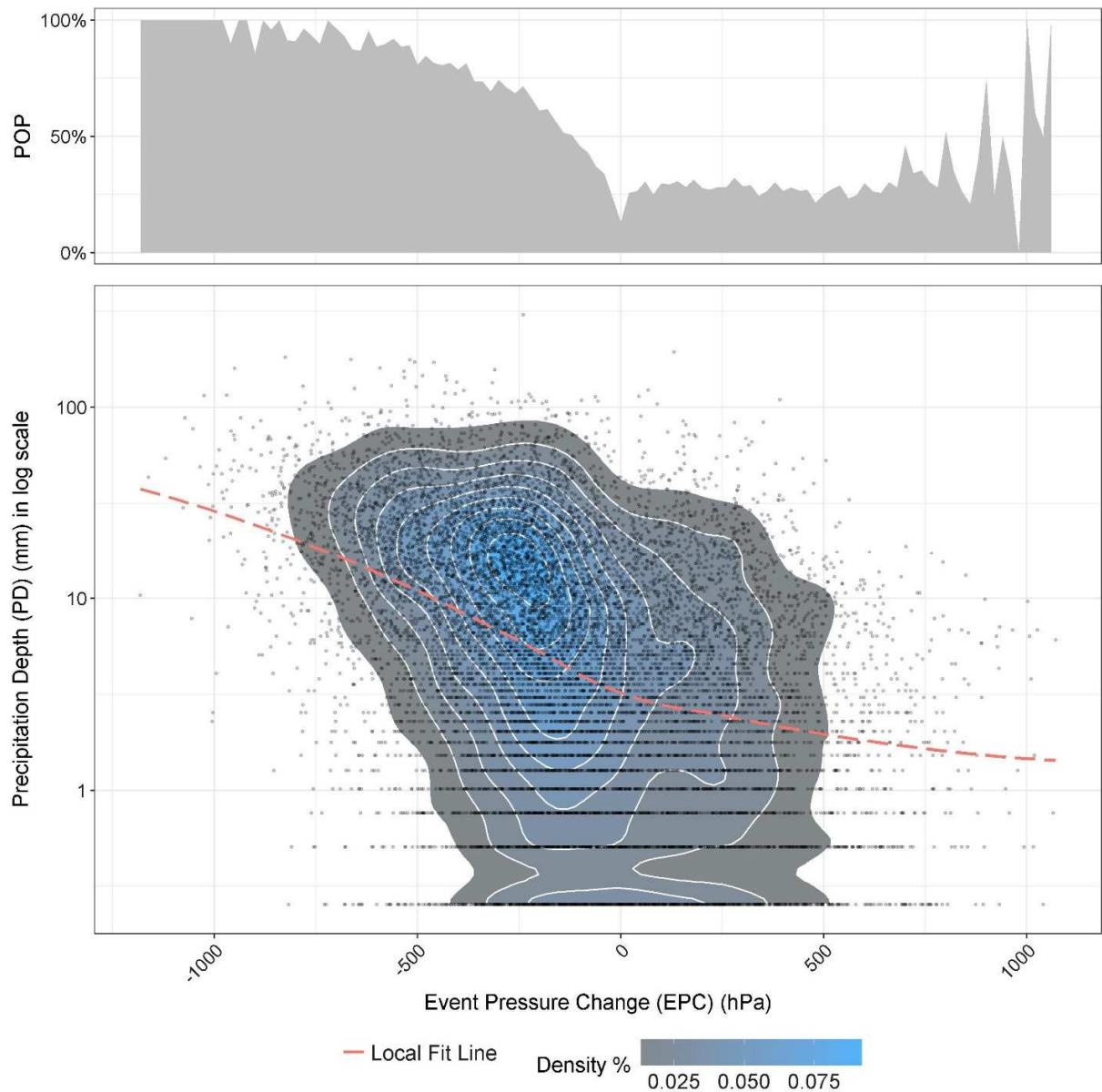
246

247

**Figure 7 Kernel density of EPC for rain triggered PCEs (green) and all PCEs (red)**



248 The POP and PD associated with EPCs are depicted graphically in Figure 8. A local fit line using loess  
249 method (Cleveland, Grosse et al. 1992) is used to highlight the correlation between POP and EPC. Note,  
250 the density plot in the lower chart reflects only the distribution of the rainy PCEs, as all dry PCEs are all  
251 laying atop the x axis (PD = 0 mm). Two distinct PCEs are divided by EPC = 0 hPa. As the absolute value  
252 of an EPC increases, the POP of DePCEs increases from 15% to 100% within 0 ~ -300 hPa, while InPCE  
253 POP increases only from 15% to about 40% within 0 ~ 820 hPa. Given that the sample size of intensive  
254 InPCEs is limited (n = 79 when EPC > 820 hPa), less confidence is associated with the POP beyond 820  
255 hPa. Falling pressure appears to be a better indicator of precipitation than increasing pressure. The  
256 highest PCE occurrence occurs at EPC values of approximately -250 hPa and PD of 20 mm. These ranges  
257 are consistent with the histogram shown in Figure 7. Similar to POP, the trend of PD versus EPC can also  
258 be divided by PCE types. For DePCEs, the PD increases along with the EPC magnitude, while for InPCEs,  
259 EPC magnitude reduces PD. Physically, InPCE appears in a stable atmosphere, which does not benefit air  
260 mass lifting and so lacks the moisture supply necessary to intensify the precipitation process as DePCE  
261 does.

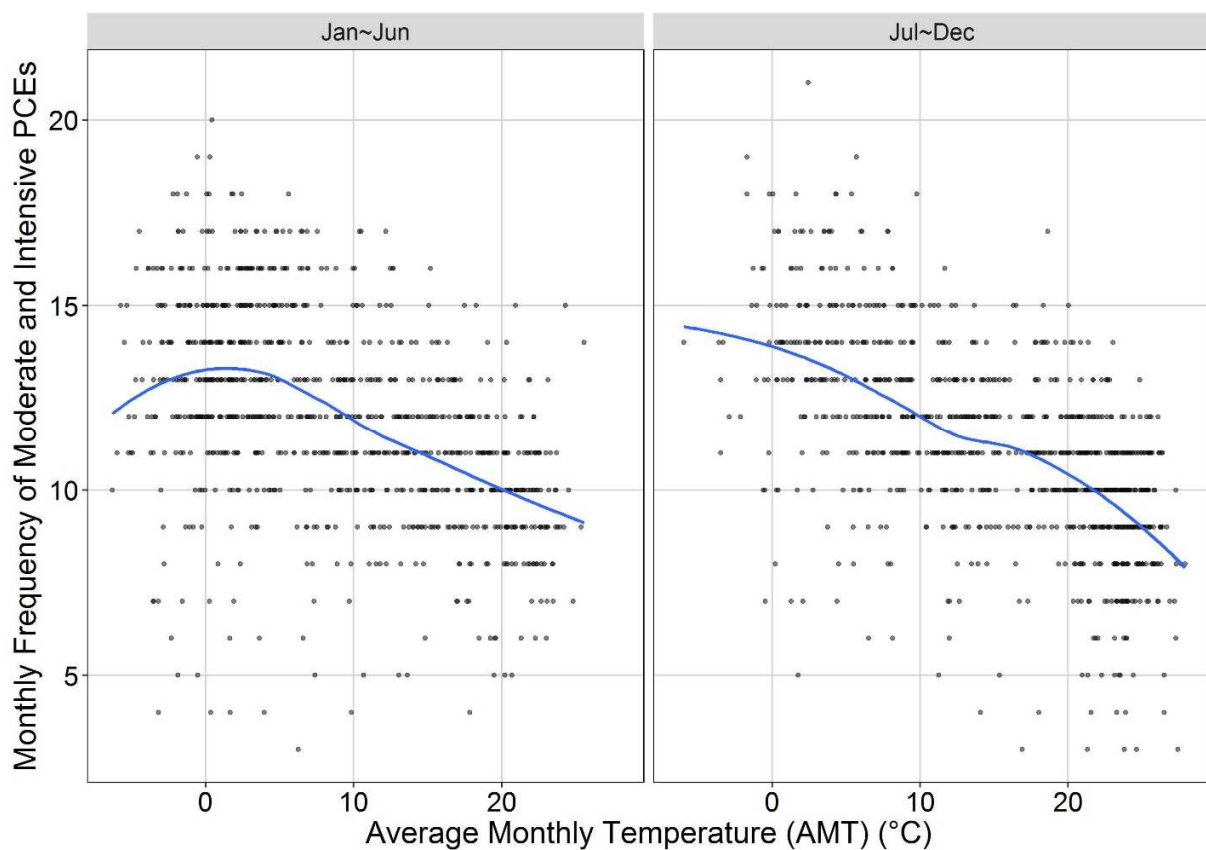


262  
263

**Figure 8 Relationship between PD and POP vs. EPC**

264 Bjerknes and Kristiania (1923) reported that the average lifetime of an air circulation system was 5.5 days,  
 265 a period that was similar in duration to the average 5.7 days of precipitation events reported in 1909 by  
 266 Defant (1921). It suggests that occurrence of air circulation and its corresponding air pressure change  
 267 could be treated as an indicator of atmosphere stability, especially for moderate and intensive events.  
 268 Since precipitation is formed due to atmospheric instability, it is important to evaluate the impact of  
 269 temperature on the atmospheric system. The monthly frequency of moderate and intensive PCEs

270 (absolute value of EPC > 90 hPa) is plotted in two half-years against AMT in Figure 9, with a local  
 271 regression line in blue. An obvious negative relationship when AMT > 0°C can be seen for both half-years.  
 272 Atmospheric systems are more stable when the weather gets cold (AMT < 0°C). This illustrates that the  
 273 atmospheric system stability, indicated by monthly frequency of moderate and intensive PCEs, is a  
 274 function of AMT, one of the GCM outputs. It should be noted that even though the occurrence becomes  
 275 low, individually PCE in high temperature is generally more intensive than low temperature.



276  
 277 **Figure 9 Association between monthly PCE frequency and AMT with local regression line (blue)**

278 To further investigate the impact of AMT on PCE and its associated precipitation characteristics, Figure  
 279 10 and 10 present the PD and POP for two halves of the year, indexed by AMT.

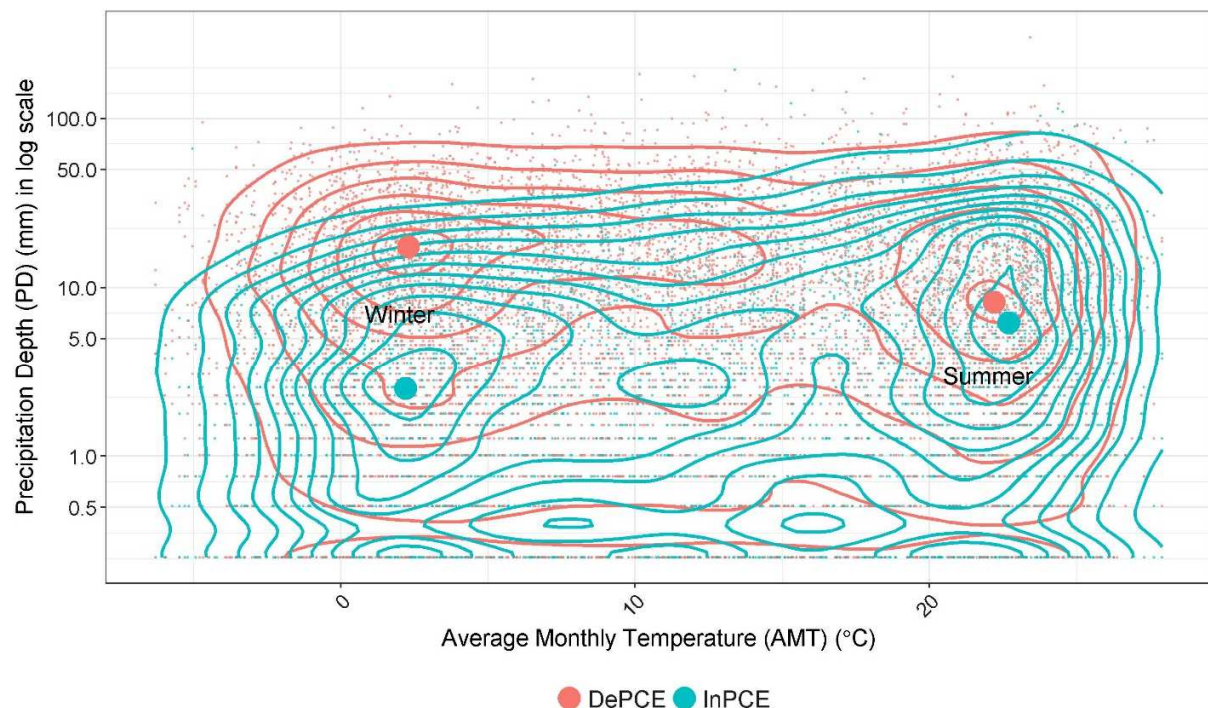
280 The relationship between PD and AMT is contoured by frequency in Figure 10 for both InPCEs and  
 281 DePCEs. Two seasonal systems (centroids), winter and summer, are visible for both PCE types. The

282 summer system is concentrated around 8 mm for DePCEs and 6 mm for InPCEs (both centroids near  
283 22°C). The difference of PD between DePCE and InPCE in summer is not pronounced since precipitation  
284 tends to be localized in the relatively stable atmospheric system, as implied by the narrow variance of air  
285 pressure. However, the opposite is true for winter system. The winter system is centered around 17.5 mm  
286 for DePCEs and 2.5 mm for InPCEs (both centroids near 2.2°C). This indicates that DePCE has a larger  
287 geographical scale effect on winter storms. The magnitude of this difference fades out as the AMT grows  
288 from winter to summer. The change in PD between winter and summer is +3.5 mm for InPCEs and -8.5  
289 for DePCEs. These differences are largely due to the seasonality of precipitation formation, with large-  
290 scale, frontal mechanisms dominating in winter, and local air convection dominating in summer.

291 Figure 11 illustrates the POP of both PCE types under different AMT conditions. The POP of DePCEs is  
292 generally higher than of InPCEs which is coincided with Figure 7 and Figure 8. For DePCEs, during both  
293 halves of a year, POP is roughly level, oscillating between 55% and 65% with some small differences in  
294 the tail regions (e.g. high and low end of AMT range). The small POP during low temperatures in the  
295 second half of the year (Jul-Dec) is not reliable, due to a limited sample size ( $n = 9$  for both InPCEs and  
296 DePCEs). However, during high temperatures, the POP decreases about 10%. This could be another  
297 impact of meso-scale summer convection storms, which generally have a tributary area much larger than  
298 the area of precipitation (Hoxit, Chappell et al. 1976, Hoxit, Chappell et al. 1976). Given that the data in  
299 the study is only from three airports, it is very likely these areas contribute to convections forming storms  
300 elsewhere. For InPCEs, during both year halves, the POP indicated is approximately 25% at the lowest  
301 temperatures and 35% at the highest. Between Jan and Jun, POP gradually rises to 35 % between 4°C and  
302 10°C, while during Jul and Dec, the increase in POP is delayed until the temperature increases from 20°C  
303 to 26°C. This observation suggests that the precipitation / pressure dynamics in the fall and spring differ  
304 somewhat from one another, although both have a similar temperature range (6°C).

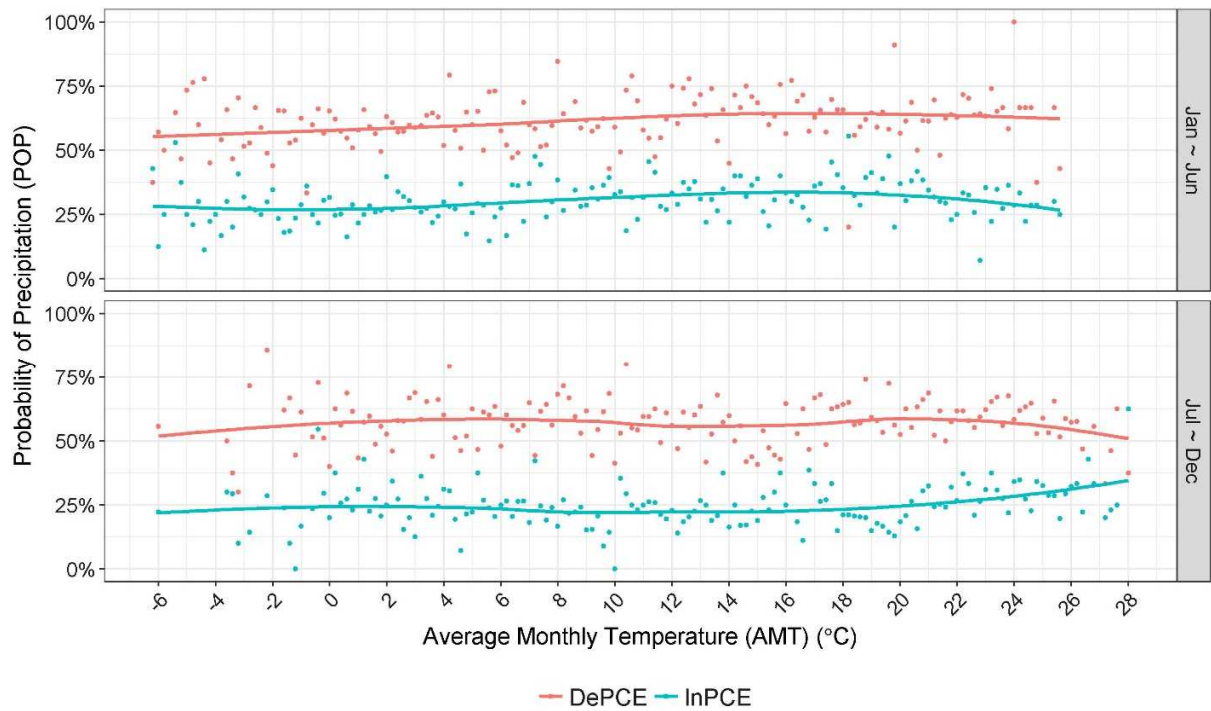
305 The PD of spring and fall are difficult to differentiate in Figure 10, since their AMTs overlap. Similar POP  
306 values are shown in Figure 11 for DePCEs, though the temperatures at which POP increases for InPCEs  
307 are slightly different. The increase in POP could be caused by warm-front frequency under different  
308 AMTs. Since warm air masses generally move to the north in spring, it is reasonable to expect stronger  
309 warm-front storms in spring than in the fall.

310



311  
312

**Figure 10 PD of different PCE types on AMT (red: DePCE, green: InPCE)**

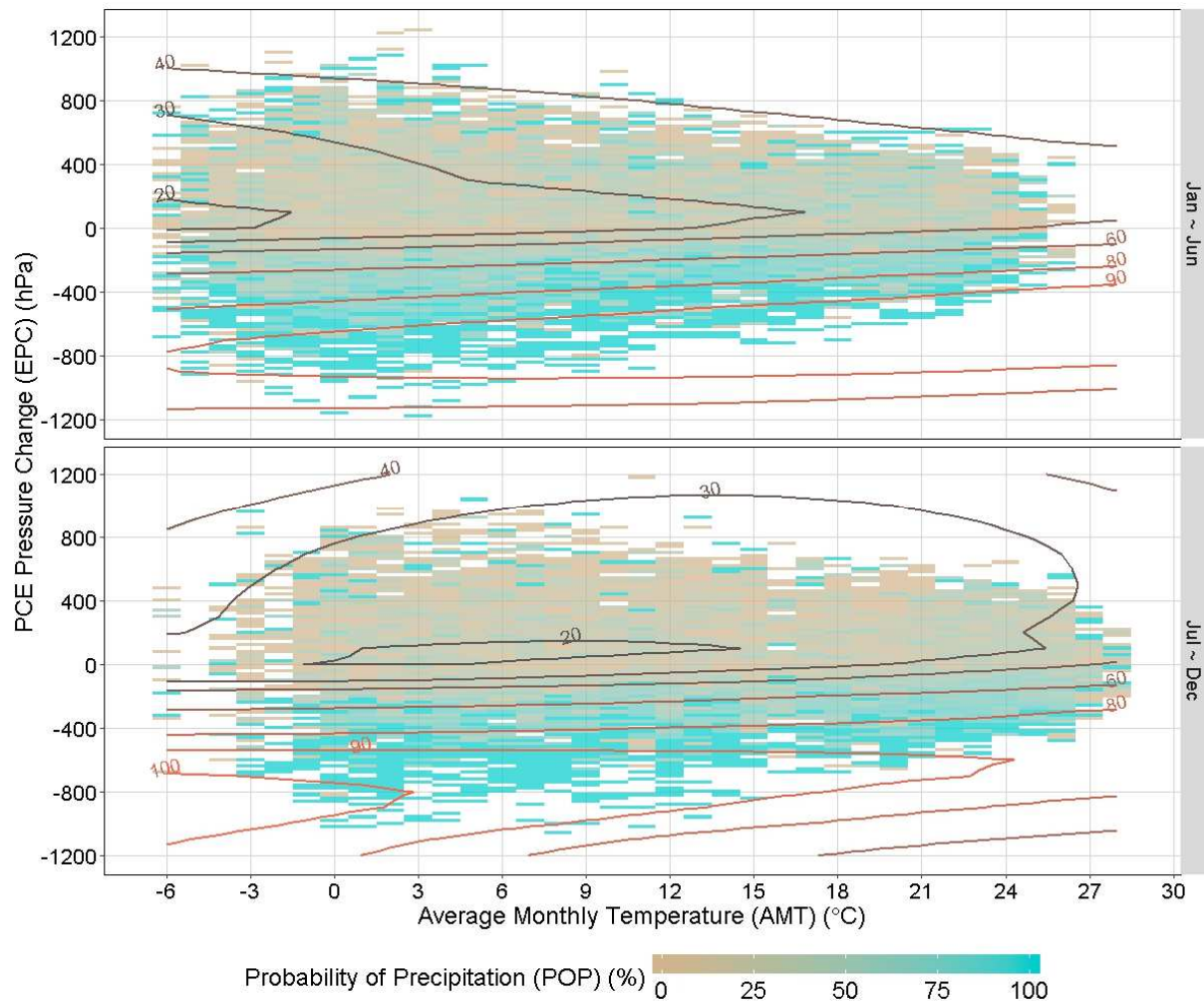


313

314 **Figure 11 POP of different PCE types on AMT in different half years (red: DePCE, green: InPCE)**

315 This analysis suggests that high POP in this geographical region is associated both with low absolute  
 316 pressure and with DePCEs. It also indicates that PCE could serve as a potential link between AMT and  
 317 POP. This relationship is plotted in Figure 12 in terms of POP and PCE against AMT, with break points in  
 318 the middle of a year. POP ranges from 0% (tan) to 100% (light blue). Generally, POP is higher in DePCEs  
 319 for the entire year. As indicated by the contours of the local regression, POP for DePCEs is highest when  
 320 EPC is near -800 hPa, regardless of the time of year. Between July and December, POP increases as  
 321 temperatures decrease. For InPCEs, EPC magnitude is positively correlated to POP, though this  
 322 correlation is more pronounced for DePCEs.





323

324

**Figure 12 PCE POP over AMT by EPC**

325 As a further investigation, we explored PD quantiles against EPC and AMT in different seasons (Figure

326 13). Three PD percentiles, 50%, 75% and 95%, are included. The relationships represented by the local

327 regression lines are colored by season. Vertically, similar to the results presented in Figure 8, PD

328 percentiles increases as the EPC drops, especially in DePCE regions. This generally holds for all PD

329 percentiles and seasons. Horizontally, PD seems to vary greatly depending on the AMT, with an

330 amplified magnitude on high percentile categories (75% and 95% quantiles). For intensive

331 (500hPa~2000hPa) and non-intensive (0hPa~500hPa) InPCEs, the all-season dash lines reflect the overall

332 relationship between PD and AMT since seasonality is not significant. When AMT is lower than 10°C, PD

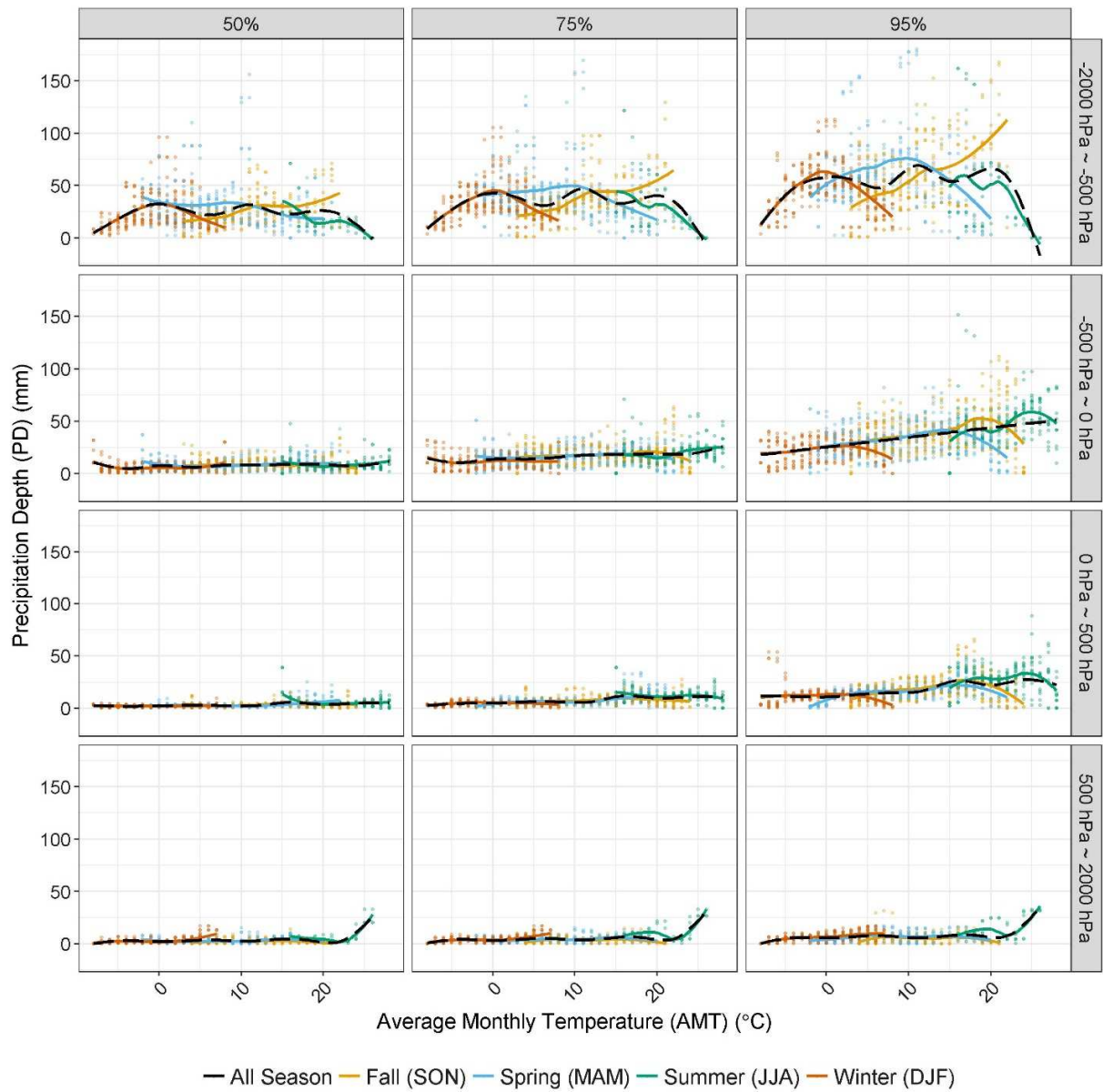
333 stays small. At temperatures above 10°C, non-intensive InPCE PD starts to increase slightly with AMT in  
334 the PD percentiles of 95%. This increase is amplified in intensive InPCEs for all PD quantiles, as shown in  
335 Figure 13, but delayed to 22°C, which almost exclusively represents summertime events. It should be  
336 noted that this amplification could be caused by the limited sample size (n = 40 for 23°C~26°C) at the  
337 corresponding AMT range and thus may not be reliable.

338 For DePCE, seasonality is more pronounced in high PD percentiles (75% and 95%) and under intensive  
339 EPC conditions. When combined with the density graph from Figure 8, non-intensive (-500hPa~0hPa)  
340 DePCEs occur more frequently than other EPC categories and thus are more important in the  
341 investigation of how PD responds to PCEs and AMT. Although not all pronounced, non-intensive  
342 DePCEs generate more precipitation when AMT is higher, obvious for PD in the 95<sup>th</sup> percentile. This  
343 trend for non-intensive DePCEs is stronger than for non-intensive InPCE in a similar AMT range. The  
344 trends for all seasons have a dropping tail for high AMTs, which could be due to shrinking sample sizes.  
345 It could also imply that extreme events (95%) are more influenced by temperature and will likely be more  
346 affected by climate change than regular events, a finding that is supported by other researchers (Allen  
347 and Ingram 2002, Trenberth, Dai et al. 2003, Allan and Soden 2008, Giorgi, Im et al. 2011).

348 Since PD is negatively associated with EPC, intensive (-2000hPa~-500hPa) DePCEs contain many extreme  
349 events. Seasonality is also more differentiable for intensive DePCEs. A monotonic positive trend between  
350 PD and AMT can be observed in fall. In winter, PD increases when the AMT is less than 0°C, and  
351 decreases for warmer temperatures. In spring, PD (except in the 95% percentile) does not obviously  
352 change until AMT is greater than 10°C. Summer shows a general monotonic decrease in PD as AMT  
353 increases. This is consistent with Shaw, Royem et al. (2011)'s findings in the NE, USA, suggesting that  
354 extreme precipitation events show a decrease in PD after 25°C during the summer.



355 The relationship between PD and AMT is important in the context of downscaling precipitation based on  
356 GCM temperature projections, the motivation for this study. AMT could generally indicate the moisture  
357 holding capacity and associated non-extreme PD trend of the CC relationship. However, at finer temporal  
358 scale or for a specific precipitation event, precipitation should be more physically related to hourly  
359 temperature (Panthou, Mailhot et al. 2014, Peleg, Marra et al. 2018). Moreover, pressure change, as a  
360 driver of precipitation investigated in this study, could impact on PD more directly than temperature and  
361 is worth to further explored.



362

363

**Figure 13 Seasonal relationship between PD, AMT and EPC in different percentiles**

364

The impacts of both AMT and EPC on precipitation characteristics (POP, PD and percentiles) in Figure 12

365

and 13 quantify the precipitation change with climate. Ban, Schmidli et al. (2015) suggest future climate

366

may not be represented by the statistics derived from present using CC-related results. In this study, it

367

might be true for the trends of precipitation characteristics in the extreme situation (e.g. an AMT or an

368

EPC not seen in the historical data, or a local scale summer convection system only shown in the point

369 source data in terms of pressure changes but not precipitation). However, the analysis in this study is not  
370 statistical based. Although the intensity of different precipitation types may vary due to divergent  
371 thermodynamic conditions across different areal, seasonal and climate conditions (Panthou, Mailhot et al.  
372 2014, Peleg, Marra et al. 2018), pressure change as a physical requirement of precipitation formation,  
373 described in this study, is independent of global warming. Thus, qualitatively, the dependences between  
374 EPC, PD and AMT will be generally held. Meanwhile, the analysis results, for observed climate, may  
375 have lower confidence under climate change, especially for local convection events, because a) the sample  
376 size of such events is underestimated in the historical data collected by point sources, such as climate  
377 stations in this study; b) the trajectory and effective area of precipitation events could change in future  
378 climate (Peleg, Marra et al. 2018).

## 379 **5. Conclusion**

380 We investigated the possibility of associating hourly precipitation / pressure data with AMT data as a  
381 preliminary analysis for generating a non-stationary, non-parametric, stochastic precipitation generator  
382 conditioning GCM monthly temperature output. Specifically, the results of this analysis answer the  
383 following two questions: 1) how PD and POP change with EPC during different types of PCE and 2) how  
384 the PD and POP of specific PCEs respond to AMT.

385 Precipitation is formed by the cooling of moist air, typically due to vertical lifting. Physically, this lifting  
386 results in reduced sea-level air pressure prior to precipitation events. This research reveals that both POP  
387 and PD are highly correlated to PCEs. It provides a more physically reliable strategy by importing  
388 pressure change for stochastic precipitation generation, either parameterized statistical type or non-  
389 parametric resampling type, to model precipitation. The dependence of precipitation characteristics (POP,  
390 PD and percentiles) on AMT and EPC (Figure 12 and 13) could also enable stochastic precipitation

391 generations to incorporate more reliable GCM AMT projections in generating non-stationary situations.  
392 For this reason, we propose a stochastic precipitation generator for generating PCE sequences  
393 conditionally, using the corresponding precipitation as an output.

394 Since the relationship between PCE and precipitation is derived from the physical precipitation formation  
395 mechanism, this kind of stochastic precipitation generator represents a much stronger and more reliable  
396 conceptual basis on which to build a model, as compared to those models barely relying on statistical  
397 assumptions. Moreover, because PCE is more strongly related to precipitation formation than coarser  
398 temporal scale temperature (e.g. monthly), it could be a reliable method for downscaling precipitation  
399 from GCM AMT projections, which are currently more trustworthy than GCM precipitation projections.  
400 Such a stochastic precipitation generator could be built by sampling PCE-associated hourly precipitation  
401 series from historical observations, and by adjusting for GCM predicted monthly temperatures.  
402 Specifically, by employing non-parametric method (Lall, Rajagopalan et al. 1996, Lall and Sharma 1996,  
403 Rajagopalan and Lall 1999), AMT projections from GCMs would be used as a reference to determine a  
404 pool of candidate PCEs under similar AMTs (i.e. a range of 6°C within which POP seasonal changes occur,  
405 as shown in Figure 11), similar to the moving window method (Rajagopalan, Lall et al. 1996). A  
406 secondary paper, specifically describing such a non-stationary non-parametric stochastic precipitation  
407 generator, will be published.

408 In all, this paper suggests a means of generating long, continuous, synthetic precipitation series from  
409 scaled-down GCM AMT projections. These series could then be used for a variety of climate change  
410 model applications, such as hydrologic and hydraulic modeling, water resource modeling, agriculture  
411 modeling.

412 **6. Acknowledgements**

413 This research was supported by the National Oceanic and Atmospheric Administration (NOAA)  
414 Supporting Regional Implementation of Integrated Climate Resilience: Consortium for Climate  
415 Risks in the Urban Northeast (CCRUN) Phase II\* (NA15OAR4310147). We thank many  
416 colleagues from Drexel University and Columbia University for the insights and expertise they  
417 provided which greatly assisted in this research. We also thank for the reviewers' comments  
418 that greatly improved the manuscript.

419

420 **References**

- 421 Adams-Selin, R. D. and R. H. Johnson (2010). "Mesoscale Surface Pressure and Temperature Features  
422 Associated with Bow Echoes." Monthly Weather Review **138**(1): 212-227.
- 423 Ahrens, C. D. (2012). Meteorology Today, Cengage Learning.
- 424 Ahrens, C. D., P. L. Jackson, C. E. J. Jackson and C. E. O. Jackson (2012). Meteorology Today: An  
425 Introduction to Weather, Climate, and the Environment, Nelson Education.
- 426 Allan, R. P. and B. J. Soden (2007). "Large discrepancy between observed and simulated precipitation  
427 trends in the ascending and descending branches of the tropical circulation." Geophysical Research  
428 Letters **34**(18).
- 429 Allan, R. P. and B. J. Soden (2008). "Atmospheric warming and the amplification of precipitation  
430 extremes." Science **321**(5895): 1481-1484.
- 431 Allen, M. R. and W. J. Ingram (2002). "Constraints on future changes in climate and the hydrologic cycle."  
432 Nature **419**(6903): 224+.
- 433 Ban, N., J. Schmidli and C. Schär (2015). "Heavy precipitation in a changing climate: Does short-term  
434 summer precipitation increase faster?" Geophysical Research Letters **42**(4): 1165-1172.
- 435 Basinger, M., F. Montalto and U. Lall (2010). "A rainwater harvesting system reliability model based on  
436 nonparametric stochastic rainfall generator." Journal of Hydrology **392**(3-4): 105-118.
- 437 Bjerknes, J. and H. S. Kristiania (1922). "Meteorological conditions for the formation of rain. ." Quarterly  
438 Journal of the Royal Meteorological Society **48**(204): 374-375.
- 439 Bjerknes, J. and H. S. Kristiania (1923). "Life cycle of cyclones and the polar front theory of atmospheric  
440 circulation. ." Quarterly Journal of the Royal Meteorological Society **49**(206): 140-141.
- 441 Cleveland, W., E. Grosse and W. Shyu (1992). Local regression models. In 'Statistical Models in S'.(Eds JM  
442 Chambers, TJ Hastie) pp. 309-376, Chapman & Hall: New York.
- 443 Dawn, S. and M. Mandal (2014). "Surface mesoscale features associated with leading convective line-  
444 trailing stratiform squall lines over the Gangetic West Bengal." Meteorology and Atmospheric Physics  
445 **125**(3): 119-133.
- 446 Defant, A. (1921). "Die Veränderungen in der allgemeinen Zirkulation der Atmosphäre in den  
447 gemäßigten Breiten der Erde." Geografiska Annaler **3**: 209-266.
- 448 Demaria, E. M. C., R. N. Palmer and J. K. Roundy (2016). "Regional climate change projections of  
449 streamflow characteristics in the Northeast and Midwest U.S." Journal of Hydrology: Regional Studies **5**:  
450 309-323.
- 451 Fowler, H. J., S. Blenkinsop and C. Tebaldi (2007). "Linking climate change modelling to impacts studies:  
452 recent advances in downscaling techniques for hydrological modelling." International Journal of  
453 Climatology **27**(12): 1547-1578.
- 454 Giorgi, F., E. S. Im, E. Coppola, N. S. Diffenbaugh, X. J. Gao, L. Mariotti and Y. Shi (2011). "Higher  
455 Hydroclimatic Intensity with Global Warming." Journal of Climate **24**(20): 5309-5324.
- 456 Groisman, P. Y., R. W. Knight, D. R. Easterling, T. R. Karl, G. C. Hegerl and V. N. Razuvaev (2005).  
457 "Trends in Intense Precipitation in the Climate Record." Journal of Climate **18**(9): 1326-1350.

458 Haberlandt, U., A. D. E. von Eschenbach and I. Buchwald (2008). "A space-time hybrid hourly rainfall  
459 model for derived flood frequency analysis." Hydrology and Earth System Sciences **12**(6): 1353-1367.

460 Hayhoe, K., C. Wake, B. Anderson, X. Z. Liang, E. Maurer, J. H. Zhu, J. Bradbury, A. DeGaetano, A. M.  
461 Stoner and D. Wuebbles (2008). "Regional climate change projections for the Northeast USA." Mitigation  
462 and Adaptation Strategies for Global Change **13**(5-6): 425-436.

463 Heneker, T. M., M. F. Lambert and G. Kuczera (2001). "A point rainfall model for risk-based design."  
464 Journal of Hydrology **247**(1): 54-71.

465 Houze, R. A., K. L. Rasmussen, M. D. Zuluaga and S. R. Brodzik (2015). "The variable nature of  
466 convection in the tropics and subtropics: A legacy of 16 years of the Tropical Rainfall Measuring Mission  
467 satellite." Reviews of Geophysics **53**(3): 994-1021.

468 Hoxit, L. R., C. F. Chappell and J. M. Fritsch (1976). "Formation of Mesolows or Pressure Troughs in  
469 Advance of Cumulonimbus Clouds." Monthly Weather Review **104**(11): 1419-1428.

470 Hoxit, L. R., C. F. Chappell and J. Michael Fritsch (1976). "Formation of mesolows or pressure troughs in  
471 advance of cumulonimbus clouds." Monthly Weather Review **104**(11): 1419-1428.

472 Hughes, K. K. and J. Mayes (2014). Understanding Weather, Taylor & Francis.

473 Johnson, F. and A. Sharma (2009). "Measurement of GCM Skill in Predicting Variables Relevant for  
474 Hydroclimatological Assessments." Journal of Climate **22**(16): 4373-4382.

475 Johnson, F. and A. Sharma (2012). "A nesting model for bias correction of variability at multiple time  
476 scales in general circulation model precipitation simulations." Water Resources Research **48**(1): n/a-n/a.

477 Kendon, E. J., D. P. Rowell, R. G. Jones and E. Buonomo (2008). "Robustness of Future Changes in Local  
478 Precipitation Extremes." Journal of Climate **21**(17): 4280-4297.

479 King, A. D., N. P. Klingaman, L. V. Alexander, M. G. Donat, N. C. Jourdain and P. Maher (2014). "Extreme  
480 Rainfall Variability in Australia: Patterns, Drivers, and Predictability." Journal of Climate **27**(15): 6035-  
481 6050.

482 Knupp, K. R. and W. R. Cotton (1985). "Convective cloud downdraft structure: An interpretive survey."  
483 Reviews of Geophysics **23**(2): 183-215.

484 Kunkel, K. E., T. R. Karl, H. Brooks, J. Kossin, J. H. Lawrimore, D. Arndt, L. Bosart, D. Changnon, S. L.  
485 Cutter, N. Doesken, K. Emanuel, P. Y. Groisman, R. W. Katz, T. Knutson, J. O'Brien, C. J. Paciorek, T. C.  
486 Peterson, K. Redmond, D. Robinson, J. Trapp, R. Vose, S. Weaver, M. Wehner, K. Wolter and D.  
487 Wuebbles (2013). "Monitoring and Understanding Trends in Extreme Storms: State of Knowledge."  
488 Bulletin of the American Meteorological Society **94**(4): 499-514.

489 Lall, U., B. Rajagopalan and D. G. Tarboton (1996). "A nonparametric wet/dry spell model for resampling  
490 daily precipitation." Water Resources Research **32**(9): 2803-2823.

491 Lall, U. and A. Sharma (1996). "A nearest neighbor bootstrap for resampling hydrologic time series."  
492 Water Resources Research **32**(3): 679-693.

493 Lenderink, G. and E. van Meijgaard (2008). "Increase in hourly precipitation extremes beyond  
494 expectations from temperature changes." Nature Geosci **1**(8): 511-514.

495 Lenderink, G. and E. van Meijgaard (2010). "Linking increases in hourly precipitation extremes to  
496 atmospheric temperature and moisture changes." Environmental Research Letters **5**(2).

497 Madden, R. A. and J. Williams (1978). "The Correlation between Temperature and Precipitation in the  
498 United States and Europe." Monthly Weather Review **106**(1): 142-147.

499 Meehl, G. A., J. M. Arblaster and C. Tebaldi (2005). "Understanding future patterns of increased  
500 precipitation intensity in climate model simulations." Geophysical Research Letters **32**(18): n/a-n/a.

501 Meehl, G. A., W. M. Washington, J. M. Arblaster, A. Hu, H. Teng, C. Tebaldi, B. N. Sanderson, J.-F.  
502 Lamarque, A. Conley, W. G. Strand and J. B. W. III (2012). "Climate System Response to External Forcings  
503 and Climate Change Projections in CCSM4." Journal of Climate **25**(11): 3661-3683.

504 Mitchell, J. F. B., T. C. Johns, M. Eagles, W. J. Ingram and R. A. Davis (1999). "Towards the Construction of  
505 Climate Change Scenarios." Climatic Change **41**(3): 547-581.

506 Neiman., P. J., F. M. Ralph., G. A. Wick., J. D. Lundquist. and M. D. Dettinger. (2008). "Meteorological  
507 Characteristics and Overland Precipitation Impacts of Atmospheric Rivers Affecting the West Coast of  
508 North America Based on Eight Years of SSM/I Satellite Observations." Journal of Hydrometeorology **9**(1):  
509 22-47.

510 Panthou, G., A. Mailhot, E. Laurence and G. Talbot (2014). "Relationship between Surface Temperature  
511 and Extreme Rainfalls: A Multi-Time-Scale and Event-Based Analysis." Journal of Hydrometeorology  
512 **15**(5): 1999-2011.

513 Peleg, N., F. Marra, S. Fatichi, P. Molnar, E. Morin, A. Sharma and P. Burlando (2018). "Intensification of  
514 convective rain cells at warmer temperatures observed from high-resolution weather radar data." Journal  
515 of Hydrometeorology **0**(0): null.

516 Räisänen, J. (2001). "CO<sub>2</sub>-Induced Climate Change in CMIP2 Experiments: Quantification of Agreement  
517 and Role of Internal Variability." Journal of Climate **14**(9): 2088-2104.

518 Rajagopalan, B. and U. Lall (1999). "A k-nearest-neighbor simulator for daily precipitation and other  
519 weather variables." Water Resources Research **35**(10): 3089-3101.

520 Rajagopalan, B., U. Lall and D. G. Tarboton (1996). "Nonhomogeneous Markov Model for Daily  
521 Precipitation." Journal of Hydrologic Engineering **1**(1): 33-40.

522 Restrepo-Posada, P. J. and P. S. Eagleson (1982). "Identification of independent rainstorms." Journal of  
523 Hydrology **55**(1): 303-319.

524 Rodriguez-Iturbe, I., D. R. Cox and V. Isham (1987). "Some Models for Rainfall Based on Stochastic Point  
525 Processes." Proceedings of the Royal Society of London. Series A, Mathematical and Physical Sciences  
526 **410**(1839): 269-288.

527 Rodriguez-Iturbe, I., D. R. Cox and V. Isham (1988). "A Point Process Model for Rainfall: Further  
528 Developments." Proceedings of the Royal Society of London. Series A, Mathematical and Physical  
529 Sciences **417**(1853): 283-298.

530 Shamir, E., S. B. Megdal, C. Carrillo, C. L. Castro, H.-I. Chang, K. Chief, F. E. Corkhill, S. Eden, K. P.  
531 Georgakakos, K. M. Nelson and J. Prietto (2015). "Climate change and water resources management in the  
532 Upper Santa Cruz River, Arizona." Journal of Hydrology **521**(Supplement C): 18-33.

533 Sharma, A. and U. Lall (1999). "A nonparametric approach for daily rainfall simulation." Mathematics and  
534 Computers in Simulation **48**(4-6): 361-371.

535 Shaw, S. B., A. A. Royem and S. J. Riha (2011). "The Relationship between Extreme Hourly Precipitation  
536 and Surface Temperature in Different Hydroclimatic Regions of the United States." Journal of  
537 Hydrometeorology **12**(2): 319-325.



538 Sorteberg, A. and N. G. KvamstØ (2006). "The effect of internal variability on anthropogenic climate  
539 projections." Tellus A 58(5): 565-574.

540 Stern, R. D. and R. Coe (1984). "A Model Fitting Analysis of Daily Rainfall Data." Journal of the Royal  
541 Statistical Society. Series A (General) 147(1): 1-34.

542 Sun, Y., S. Solomon, A. Dai and R. W. Portmann (2007). "How often will it rain?" Journal of Climate 20(19):  
543 4801-4818.

544 Trenberth, K. E. (1998). "Atmospheric moisture residence times and cycling: Implications for rainfall rates  
545 and climate change." Climatic Change 39(4): 667-694.

546 Trenberth, K. E. (2011). "Changes in precipitation with climate change." Climate Research 47(1-2): 123-138.

547 Trenberth, K. E., A. Dai, R. M. Rasmussen and D. B. Parsons (2003). "The changing character of  
548 precipitation." Bulletin of the American Meteorological Society 84(9): 1205-+.

549 Trenberth, K. E. and D. J. Shea (2005). "Relationships between precipitation and surface temperature."  
550 Geophysical Research Letters 32(14).

551 Urbana-Champaign, W. W. W. a. t. U. o. I. a. (2010). "Occluded Front." from  
552 <http://ww2010.atmos.uiuc.edu/%28Gh%29/guides/mtr/af/frnts/ofdef.rxml>.

553 USGCRP (2017). Climate Science Special Report: Fourth National Climate Assessment, Volume I. D. J.  
554 Wuebbles, D. W. Fahey, K. A. Hibbard et al. U.S. Global Change Research Program, Washington, DC,  
555 USA: 470 pp.

556 Wasko, C., A. Pui, A. Sharma, R. Mehrotra and E. Jeremiah (2015). "Representing low-frequency  
557 variability in continuous rainfall simulations: A hierarchical random Bartlett Lewis continuous rainfall  
558 generation model." Water Resources Research 51(12): 9995-10007.

559 Wasko, C. and A. Sharma (2017). "Continuous rainfall generation for a warmer climate using observed  
560 temperature sensitivities." Journal of Hydrology 544(Supplement C): 575-590.

561 Wasko, C., A. Sharma and F. Johnson (2015). "Does storm duration modulate the extreme precipitation-  
562 temperature scaling relationship?" Geophysical Research Letters 42(20): 8783-8790.

563 Westra, S., L. V. Alexander and F. W. Zwiers (2013). "Global Increasing Trends in Annual Maximum  
564 Daily Precipitation." Journal of Climate 26(11): 3904-3918.

565 Wilks, D. S. (1998). "Multisite generalization of a daily stochastic precipitation generation model." Journal  
566 of Hydrology 210(1): 178-191.

567 Wilks, D. S. (2010). "Use of stochastic weather generators for precipitation downscaling." Wiley  
568 Interdisciplinary Reviews-Climate Change 1(6): 898-907.

569 Wilks, D. S. and R. L. Wilby (1999). "The weather generation game: a review of stochastic weather  
570 models." Progress in Physical Geography 23(3): 329-357.

571 Zhao, W. and M. A. K. Khalil (1993). "The Relationship between Precipitation and Temperature over the  
572 Contiguous United States." Journal of Climate 6(6): 1232-1236.

573 Zvervaev, I. I. and R. P. Allan (2005). "Water vapor variability in the tropics and its links to dynamics and  
574 precipitation." Journal of Geophysical Research: Atmospheres 110(D21): n/a-n/a.

575